Dalton Transactions

ROYAL SOCIETY OF CHEMISTRY

PAPER

View Article Online
View Journal | View Issue

Cite this: *Dalton Trans.*, 2025, **54**, 1454

Synthesis, cytotoxicities, structural properties and comparison of dihalogeno-substituted-thiosemicarbazone ligands and mixed-ligand Ni(II) complexes†

Elif Avcu Altiparmak, [a] Güneş Özen Eroğlu, [b] Namık Özdemir, [c] Serap Erdem Kuruca [d,e] and Tülay Bal Demirci *[a]

Received 1st October 2024,
Accepted 16th November 2024

DOI: 10.1039/d4dt02774d

rsc.li/dalton

Three novel mixed-ligand Ni(II) complexes were synthesized from a 3,5-dihalogenosalicylaldehyde-*S*-methyl isothiosemicarbazone ligand (3,5-dichloro for **Complex I**, 3,5-dibromo for **Complex II**, and 3,5-diiodo for **Complex III**) and diethanolamine. The synthesized compounds were characterized by elemental analysis, FT-IR, UV-Vis and ^{1}H-NMR spectroscopy. Solid-state structures of **Complex I** and **Complex II** were determined by the single-crystal X-ray diffraction technique. Both the complexes were found to have a distorted square planar geometry, with coordination of azomethine nitrogen, phenolate oxygen, terminal amine of the thiosemicarbazone ligand and amine nitrogen of diethanolamine. The cytotoxic effects of the ligands and the complexes were evaluated against two different types of cancer cells (THP-1 human leukaemia monocytic cell line and MDA-MB-231 aggressive breast cancer cell line) and healthy cells (HUVEC human umbilical vein endothelial cell line) by using the MTT method. The findings demonstrated that the chloro-derivatives exhibited better efficacy compared to cisplatin in targeting the monocytic leukemia cell line while displaying reduced toxicity towards healthy cells.

1. Introduction

On a global scale, cancer has consistently been a prominent cause of illness and death for populations. The World Health Organization (WHO) maintains that cancer causes a major part of annual mortality. The discovery of the biological activity of cisplatin and its application to cancer treatment brought considerable attention to the use of metal complexes in cancer therapy.[1] Cisplatin is a highly effective cancer drug, but it has shown cytostatic resistance and severe side effects.[2] It is important to synthesize novel compounds with anticancer activity due to the increasing incidences of anticancer drug resistance in the past few decades. Drug resistance is a significant challenge in cancer treatment, and can arise from many mechanisms, such as changes in drug metabolism, activation of alternative signalling pathways, and genetic mutations.[3–5] Some studies have shown that metal complexes increase and diversify the biological activities of organic compounds.[6,7] Therefore, metal complexes of drug-candidate compounds have also become an important subject of anticancer investigations.

Thiosemicarbazones and their metal complexes are well-known for their wide range of biological activities such as cytotoxic, antiviral, antidiabetic, antibacterial, antioxidant, antitumoral, anti-inflammatory, enzyme inhibition, DNA binding, antimalarial and antimicrobial.[8–19] The therapeutic activity of thiosemicarbazone compounds can be modified or enhanced by metal complexation.[7,20,21] The role of nickel in bioinorganic chemistry has been rapidly expanded since the discovery that urease is a nickel enzyme in 1975.[22] Nickel(II) ions can be found in biological systems, and they play essential roles in certain organisms.[23] Various biological applications of Ni(II) complexes of thiosemicarbazones have been described, such as anticancer, antimalarial, antimicrobial, antiproliferative, CT-DNA binding, BSA-protein binding, and antioxidant activities.[21,24–31]

[a]*Department of Chemistry, Engineering Faculty, Inorganic Chemistry Department, Istanbul University-Cerrahpasa, 34320 Istanbul, Turkiye.*
E-mail: tulaybal@iuc.edu.tr
[b]*Department of Molecular Medicine, Aziz Sancar Institute of Experimental Medicine, Istanbul University, 34093 Istanbul, Turkiye*
[c]*Department of Physics, Faculty of Art and Science, Ondokuz Mayis University, 55139 Samsun, Turkiye*
[d]*Department of Physiology, Faculty of Medicine, Istanbul University, 34390 Istanbul, Turkiye*
[e]*Department of Physiology, Faculty of Medicine, Istanbul Atlas University, 34408 Istanbul, Turkiye*

† Electronic supplementary information (ESI) available. CCDC 2288067–2288069. For ESI and crystallographic data in CIF or other electronic format see DOI: https://doi.org/10.1039/d4dt02774d

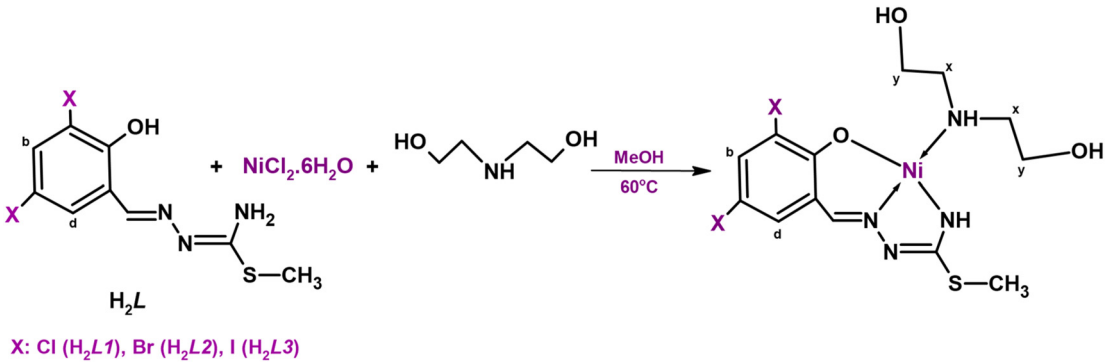

Scheme 1 Synthesis of the complexes.

In this work, three novel mixed-ligand thiosemicarbazone Ni(II) complexes (**Complex I**, **Complex II** and **Complex III**), including a 3,5-dihalogeno-salicylaldehyde-*S*-methyl-isothiosemicarbazone ligand (Cl, Cl for H_2L1, Br, Br for H_2L2 and I, I for H_2L3) with diethanolamine molecules, were synthesized (Scheme 1). Structural characterization was performed by elemental analysis, and IR, ^{1}H-NMR and UV-Vis spectroscopy and the structures of the complexes were determined by single-crystal X-ray analysis. The cytotoxic activities of the compounds were investigated against the MDA-MB-231 aggressive breast cancer cell line and THP-1 human leukemia monocytic cell line by using the MTT method.

2. Results and discussion

2.1. Synthesis and physical properties

Condensation reactions between *S*-methyl-isothiosemicarbazide and 3,5-dihalogeno-substituted salicylaldehyde (Cl for ***L1***, Br for ***L2***, and I for ***L3***) resulted in ligands H_2L1, H_2L2 and H_2L3. All ligands were very soluble in methanol, ethanol, dichloromethane, diethylether, chloroform, DMF and DMSO.

The mixed ligand complexes were synthesized by the reaction of equimolar amounts (1 : 1 : 1) of the ligand, $NiCl_2{\cdot}6H_2O$ and diethanolamine. **Complex I** and **Complex II**, red crystal products, were soluble in dichloromethane, diethyl ether, chloroform, DMF and DMSO and poorly soluble in alcohols. **Complex III** was obtained in an amorphous powder form and had poorer solubility compared to the other complexes. The complexes were characterized by elemental analysis, FT-IR, UV-Vis and ^{1}H-NMR spectroscopic methods and the structure of products in a crystalline form was determined by X-ray diffraction.

Magnetic measurements of complexes showed that they were diamagnetic and in a square-planar structure, whereas the molar conductivity values of the complexes indicated their non-electrolytic behaviour.

2.2. Structural characterization

UV-Vis spectra of the ligands showed five intense absorptions in the range of 208–350.50 nm which can be attributed to the n → σ*, π → π* and n → π* transitions of the phenol, aromatic, azomethine, and thioamide groups of the thiosemicarbazone molecules.[32]

In the UV-vis spectra of **Complexes I**, **II**, and **III** the bands in the 204.50–215.50 nm range were related to the π → π* transitions due to the aromatic rings of the thiosemicarbazone group, the bands in the 238.50–243, 300.50–312.50 and 360–384 nm ranges can be attributed to the n → π* transitions of the azomethine groups and π → π* transitions of the thioamide groups of the structures. The bands associated with the thioamide group exhibited a shift of approximately 40 nm following complex formation and a decrease in the intensity of the band corresponding to the azomethine group because of coordinate covalent bonding through the imine nitrogen. In the UV-vis spectra of the complexes, transition peaks around 210 nm expected for diethanolamine could not be clearly distinguished from others owing to the presence of thiosemicarbazone peaks in this range. The electronic spectra of the complexes provided indications that they exhibit similar structures.

The infrared spectra of the compounds supported the formation of the expected structures. In the IR spectra of H_2L1, H_2L2 and H_2L3, phenolic ν(OH) bands, ν(NH) stretching bands and $\delta(NH_2)$ intraplanar bending bands were observed at 3481–3460, 3281–3153 and 1653–1623 cm^{-1}, respectively. The vibrations of the terminal amine group in the ligands were observed at specific frequencies. The presence of imine (C=N) bands at 1609 and 1576 cm^{-1} in the spectrum of H_2L1 (at 1629 and 1595 cm^{-1} for H_2L2 and at 1619 and 1593 cm^{-1} for H_2L3) proved that the aldehyde group was connected to the thiosemicarbazide. The ν(C–S) vibrations of the *S*-methyl group were seen at 734 cm^{-1}, also.

On examining the spectra of **complexes I**, **II**, and **III**, the peaks belonging to the hydroxyl groups of the diethanolamine molecule coordinated to the metal atom were observed at 3481, 3370 and 3419 cm^{-1}, while those corresponding to the NH vibrations of the coligand diethanolamine were observed at 3244, 3271 and 3211 cm^{-1}, respectively. The stretching (C=N) bands of the complexes were observed in the range of 1610–1560 cm^{-1}, and these bands exhibited a lower frequency compared to the ligands due to the coordination through the nitrogen atom of the imine groups.

In the 1H-NMR spectra of the ligands, two signals corresponding to the *cis–trans* isomers of hydroxyl groups were observed at 12.59 and 11.81 ppm for **H_2L1**, 12.58 and 10.76 ppm for **H_2L2** and 12.79 and 12.15 ppm for **H_2L3**. The protons of the imine groups exhibited distinct signals indicating the presence of *syn–anti* isomers at chemical shifts of 8.45 and 8.35 ppm for **H_2L1**, 8.56 and 8.35 ppm for **H_2L2** and 9.88 and 8.24 ppm for **H_2L3**. While a broad singlet was observed belonging to the amine group at 7.20 ppm in the spectrum of the **H_2L1**, two broad singlets were seen at 8.15 and 7.35 ppm in a ratio of 1 : 1 *cis*/*trans* for **H_2L2** and at 8.34 and 7.18 ppm in a ratio of 1 : 1 *cis*/*trans* for **H_2L3**. The singlet peaks corresponding to the *S*-methyl groups of the ligands were observed at chemical shifts of 2.47 and 2.39 ppm for **H_2L1**, 2.66 and 2.48 ppm for **H_2L2** and 2.45 and 2.37 ppm for **H_2L3** in a 1 : 2 isomer ratio. In the spectra of the complexes, the proton of the imine groups was seen as a singlet at 8.00, 7.99 and 7.91 ppm for **Complex I**, **Complex II** and **Complex III**, respectively. The complexes exhibited a broad singlet of NH protons at 2.39 and 2.40 ppm and a prominent singlet of *S*-methyl groups was observed at 2.37 ppm. The signals of the diethanolamine molecule coordinating the structure of the complexes as a secondary ligand were also clearly seen in the spectra. In the spectra of the complexes, the hydroxyl signals of the co-ligand were observed as broad singlets at 2.95 and 2.40 ppm for **Complex I**, 3.85 and 3.00 ppm for **Complex II** and 3.52 and 3.00 ppm for **Complex III**. The signals of the $-CH_2-$ protons of diethanolamine molecules were observed with a similar character in the range of 4.99–4.26 ppm for all complexes. While the imine and d and b protons of the thiosemicarbazone molecules were sharply visible, the NH and OH peaks were almost 0.1 ppm wide due to the acidic character given to the structures by diethanolamine molecules. The broadening noticed in the peaks of these protons was also a consequence of intramolecular hydrogen bonding.[33]

2.3. Crystal structures

Crystal data, data collection and structure refinement details are presented in Table 1.

The molecular structure of **H_2L1** is shown in Fig. 1 while selected bond lengths and angles are presented in Table 2. The ligand crystallizes in a triclinic lattice with the space group $P\bar{1}$.

The molecule shows a *Z* configuration with respect to the N2═C8 bond. This is confirmed by the N1–N2–C8–S1 and N1–N2–C8–N3 torsion angles of 3.3(3) and −177.78(19)°, respectively. The N1═C7 and N2═C8 bond distances are 1.275(3) and 1.300(3), respectively, indicating that the bond distances are nearly the same as that of the C═N double bond [1.28 Å].[34] The N3–C8 and N1–N2 bond distances of 1.342(3) and 1.387(2) Å, respectively, correspond to single bond lengths, confirming that the free ligand exists in its amido form. These bonds are consistent with those previously reported for other isothiosemicarbazone organic compounds.[35–41]

Table 1 Crystal data and structure refinement parameters for **H_2L1**, **Complex I** and **Complex II**

Parameters	[**H_2L1**]	**Complex I**	**Complex II**
CCDC depository	2288067	2288068	2288069
Color/shape	Dark red/prism	Dark red/prism	Dark red/prism
Chemical formula	$C_9H_9Cl_2N_3OS$	$[Ni(C_9H_7Cl_2N_3OS)(C_4H_{11}NO_2)]$	$[Ni(C_9H_7Br_2N_3OS)(C_4H_{11}NO_2)]$
Formula weight	278.15	439.98	528.90
Temperature (K)	296(2)	296(2)	296(2)
Wavelength (Å)	0.71073 Mo Kα	0.71073 Mo Kα	0.71073 Mo Kα
Crystal system	Triclinic	Monoclinic	Monoclinic
Space group	$P\bar{1}$ (No. 2)	$P2_1/c$ (No. 14)	$P2_1/c$ (No. 14)
Unit cell parameters			
a, *b*, *c* (Å)	6.2672(5), 7.9274(6), 12.4219(9)	12.3415(8), 10.1900(6), 15.4159(11)	12.6900(8), 10.2688(5), 15.4499(12)
α, *β*, *γ* (°)	82.624(6), 78.692(6), 76.836(6)	90, 110.924(5), 90	90, 111.571(5), 90
Volume (Å^3)	587.00(8)	1810.9(2)	1872.3(2)
Z	2	4	4
$D_{calc.}$ (g cm^{-3})	1.574	1.614	1.876
μ (mm^{-1})	0.712	1.501	5.435
F_{000}	284	904	1048
Crystal size (mm^3)	0.70 × 0.56 × 0.53	0.61 × 0.26 × 0.14	0.74 × 0.33 × 0.21
Diffractometer	STOE IPDS II	STOE IPDS II	STOE IPDS II
Measurement method	*ω* scan	*ω* scan	*ω* scan
Index ranges	$-8 \le h \le 8$, $-10 \le k \le 10$, $-16 \le l \le 14$	$-13 \le h \le 16$, $-13 \le k \le 12$, $-20 \le l \le 20$	$-15 \le h \le 16$, $-12 \le k \le 13$, $-20 \le l \le 20$
θ range for data collection (°)	$2.649 \le \theta \le 27.693$	$2.449 \le \theta \le 27.750$	$2.438 \le \theta \le 27.760$
Reflections collected	6646	11 650	15 384
Independent/observed reflections	2751/2285	4227/2528	4379/3039
$R_{int.}$	0.1283	0.0612	0.0812
Refinement method	Full-matrix least-squares on F^2	Full-matrix least-squares on F^2	Full-matrix least-squares on F^2
Data/restraints/parameters	2751/0/147	4227/0/220	4379/0/220
Goodness-of-fit on F^2	1.067	0.944	1.030
Final *R* indices [$I > 2\sigma(I)$]	$R_1 = 0.0514$, w$R_2 = 0.1499$	$R_1 = 0.0509$, w$R_2 = 0.0867$	$R_1 = 0.0506$, w$R_2 = 0.1057$
R indices (all data)	$R_1 = 0.0599$, w$R_2 = 0.1566$	$R_1 = 0.1032$, w$R_2 = 0.1002$	$R_1 = 0.0825$, w$R_2 = 0.1171$
$\Delta\rho_{max.}$, $\Delta\rho_{min.}$ (e Å^{-3})	0.52, −0.34	0.41, −0.23	0.83, −0.55

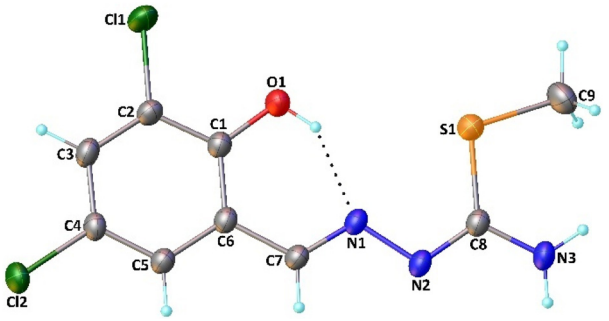

Fig. 1 Molecular structure of H_2L1 with the atom numbering. Thermal ellipsoids are shown at the 30% probability level. The intramolecular interaction is represented by dotted lines.

Table 2 Selected geometric parameters for H_2L1, **Complex I** and **Complex II**

Parameters	[H_2L1]	**Complex I**	**Complex II**
Bond lengths (Å)			
Ni1–O1	—	1.824(2)	1.830(3)
Ni1–N1	—	1.842(3)	1.855(3)
Ni1–N3	—	1.834(3)	1.844(4)
Ni1–N4	—	*1.953(3)*	1.968(3)
S1–C8	1.751(2)	1.757(3)	1.764(5)
S1–C9	1.792(3)	1.780(4)	1.795(6)
O1–C1	1.340(3)	1.302(4)	1.302(5)
N1–N2	1.387(2)	1.408(4)	1.410(5)
N1–C7	1.275(3)	1.291(4)	1.296(6)
N2–C8	1.300(3)	1.325(4)	1.333(6)
N3–C8	1.342(3)	1.311(4)	1.312(6)
N4–C10	—	1.487(4)	1.494(6)
N4–C12	—	1.474(5)	1.484(6)
Bond angles (°)			
O1–Ni1–N1	—	95.65(12)	95.54(14)
O1–Ni1–N3	—	177.96(13)	177.72(15)
O1–Ni1–N4	—	87.35(12)	87.51(14)
N1–Ni1–N3	—	82.34(13)	82.35(16)
N1–Ni1–N4	—	174.26(12)	174.25(16)
N3–Ni1–N4	—	94.68(13)	94.66(16)
C8–S1–C9	104.28(13)	103.5(2)	104.1(2)
S1–C8–N2	121.16(16)	120.3(3)	120.5(3)
S1–C8–N3	120.30(18)	118.2(3)	118.0(3)
O1–C1–C2	118.9(2)	119.2(3)	119.4(4)
O1–C1–C6	122.80(19)	124.2(3)	124.4(4)
N1–C7–C6	120.7(2)	124.3(3)	124.3(4)
N2–N1–C7	115.52(18)	116.4(3)	116.7(4)
N1–N2–C8	111.57(18)	106.6(3)	106.8(3)
N2–C8–N3	118.5(2)	121.4(3)	121.5(4)
C10–N4–C12	—	110.3(3)	110.1(4)
Torsion angles (°)			
O1–C1–C6–C7	2.8(3)	0.2(3)	1.3(5)
N2–N1–C7–C6	−178.55(18)	−178.2(3)	−178.5(4)
C7–N1–N2–C8	−178.36(18)	−179.9(3)	179.3(4)
N1–N2–C8–S1	3.3(3)	−178.0(2)	−178.0(3)
N1–N2–C8–N3	−177.78(19)	−0.4(5)	0.2(6)
N2–C8–S1–C9	−175.2(2)	−14.0(3)	−12.6(5)
N3–C8–S1–C9	5.9(2)	168.3(3)	169.2(4)

In the molecular structure of H_2L1, an intramolecular O–H···N contact (Fig. 1) leads to the formation of a six-membered ring with a graph-set descriptor $S(6)$.[42] In the crystal structure, atom N3 in the molecule at (x, y, z) acts as a hydrogen-bond donor to atom N2 in the molecule at ($-x$, $-y$ + 1, $-z$), forming a centrosymmetric $R_2^2(8)$ dimer. The dimers are linked by weak N–H···Cl interactions. In these interactions, atom N3 in the molecule at (x, y, z) acts as a hydrogen-bond donor to atom Cl2 in the molecule at (x − 2, y + 1, z). These interactions together with the N–H···N hydrogen bonds generate a second ring motif with a graph-set descriptor of $R_2^4(20)$. Propagation of these interactions by translation and inversion then leads to the formation of a two-dimensional network (Fig. 2).

The molecular structures of **Complex I** and **Complex II** are shown in Fig. S1 and S2,† respectively, while selected bond lengths and angles are given in Table 2. Both the complexes crystallizing in a monoclinic lattice with the space group $P2_1/c$ have almost the same composition, and the difference originates from the presence of different halogen atoms at the 3- and 5-positions of the phenyl ring of the isothiosemicarbazone ligand in the structures. The structures showed that the thiosemicarbazone ligand is coordinated to Ni(II) in a tridentate fashion, forming six- and five-membered chelate rings. As the bite angles corresponding to the formation of the five-membered rings are slightly contracted (~82°), the others corresponding to the formation of the six-membered rings are slightly enlarged (~96°). In **Complex I** and **Complex II**, the Ni atoms are located in a distorted square-planar fashion and surrounded by the tridentate ONN ligand and diethanolamine. The Ni1–O1, Ni1–N1, Ni1–N3 and Ni1–N4 bond distances are 1.824(2), 1.842(3), 1.834(3) and 1.953(3) Å for **Complex I** and 1.830(3), 1.855(3), 1.844(4) and 1.968(3) Å for **Complex II**, respectively, which are well comparable with those found for similar Ni(II) complexes.[41,43–46] The Z conformation of H_2L1 changes to the E conformer by rotation about the N2=C8 bond upon coordination to the metal. Due to the coordination, the N1–N2, N1–C7 and N2–C8 bond lengths in the complexes increase, while the O1–C1 and N3–C8 bond lengths decrease. For quantitative evaluation of the extent of distortion around the metal centers, the four-coordinate structural indices τ_4 [47] and τ_4' [48] were employed;

$$\tau_4 = \frac{360^\circ - (\alpha + \beta)}{360^\circ - 2\theta} \quad \tau_4' = \frac{\beta - \alpha}{360^\circ - \theta} + \frac{180^\circ - \beta}{180^\circ - \theta}$$

where α and β ($\beta < \alpha$) are the two greatest valence angles and θ is the ideal tetrahedral angle (109.5°). The τ_4 and τ_4' values for ideal square-planar and tetrahedral coordination spheres are 0 and 1, respectively. The calculated τ_4 and τ_4' geometry indices are 0.06 and 0.04 for **Complex I** and 0.06 and 0.05 for **Complex II**, indicating a slightly distorted square-planar geometry.

In the molecular structure of the complexes, no intramolecular interactions are observed. However, the complexes show the same supramolecular features with small dimensional differences. In the crystal structures of both complexes, atoms O3 and N3 in the molecule at (x, y, z) act as a hydrogen-bond donor to atoms O2 and O3 in the molecule at ($-x$ + 1, $-y$, $-z$ + 1), forming centrosymmetric $R_2^2(16)$ and $R_2^2(14)$ dimers, respectively (Fig. 3 and 4). The dimers are linked by

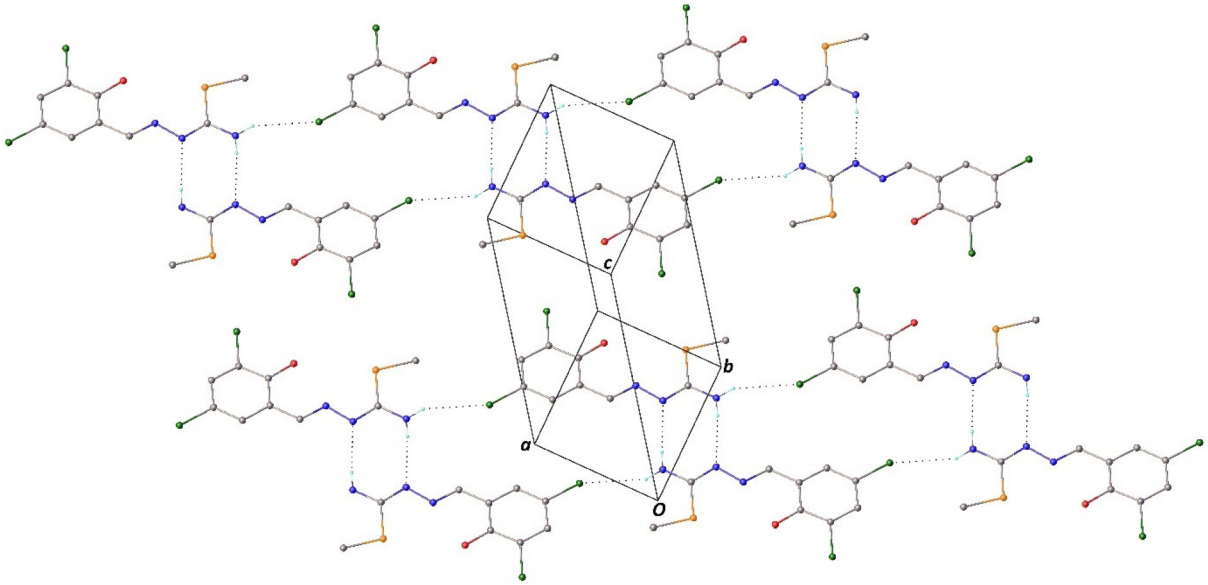

Fig. 2 Part of the crystal structure of H_2L1, showing the formation of $R_2^2(8)$ and $R_2^4(20)$ rings. The intermolecular interactions are represented by dotted lines, and H atoms not involved in the motifs shown have been omitted for clarity.

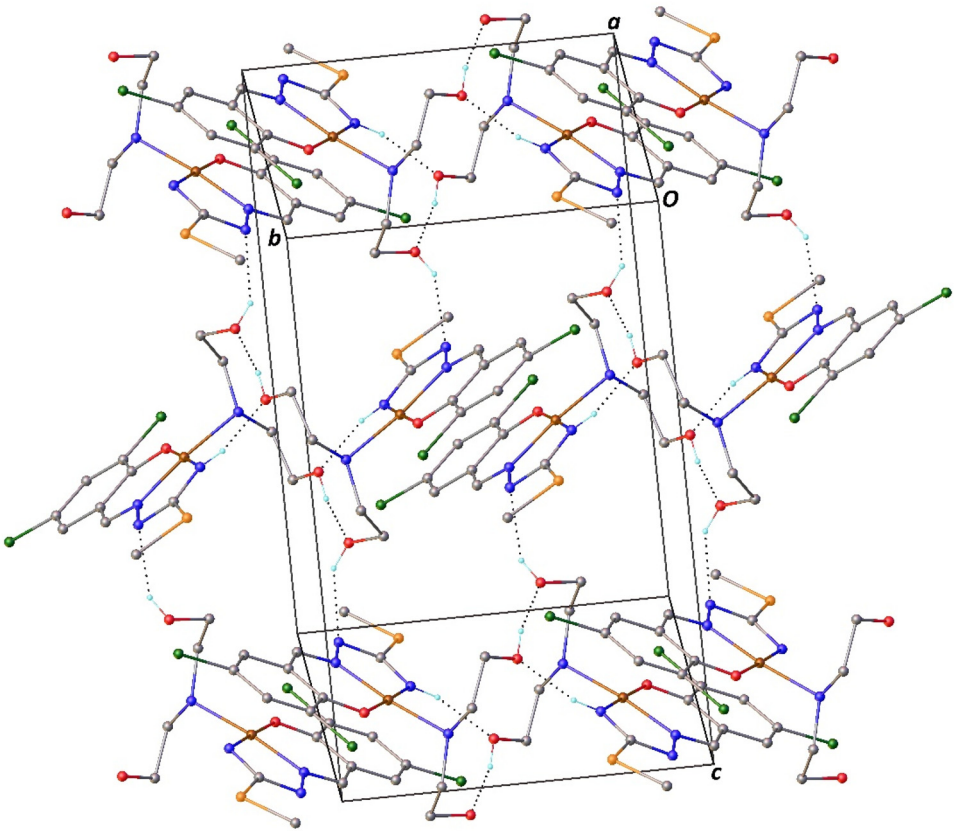

Fig. 3 Part of the crystal structure of **Complex I**, showing the intermolecular hydrogen bonds represented by dotted lines. H atoms not involved in the interactions have been omitted for clarity.

O–H···N interactions to form the two-dimensional network. In this interaction, atom O2 in the molecule at (x, y, z) acts as a hydrogen-bond donor to atom N2 in the molecule at (x, $-y + 1/2$, $z - 1/2$) for **Complex I** and in the molecule at (x, $-y + 1/2$, $z + 1/2$) for **Complex II**. Full details of the hydrogen-bonding geometries are given in Table 3.

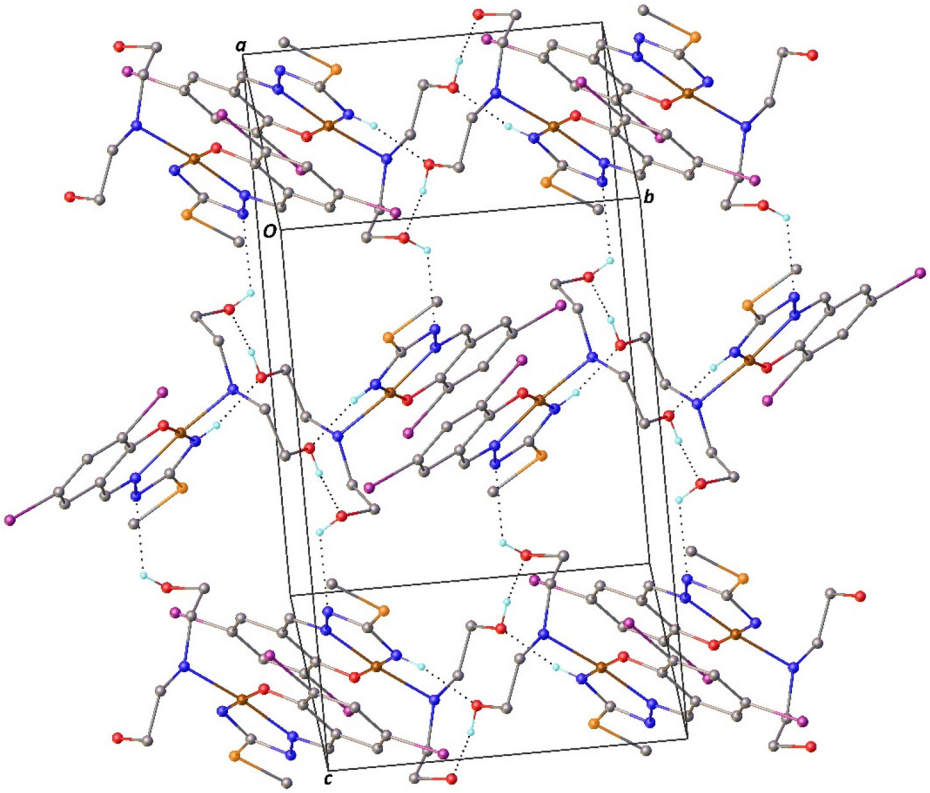

Fig. 4 Part of the crystal structure of **Complex II**, showing the intermolecular hydrogen bonds represented by dotted lines. H atoms not involved in the interactions have been omitted for clarity.

Table 3 Hydrogen bonding geometry for H_2***L1***, **Complex I** and **Complex II**

D–H···A	D–H (Å)	H···A (Å)	D···A (Å)	D–H···A (°)
H_2*L1*				
O1–H1···N1	0.82	1.90	2.618(3)	146
N3–H3A···N2^{i}	0.86	2.24	3.072(3)	164
N3–H3B···Cl2^{ii}	0.86	2.86	3.599(2)	145
Complex I				
O2–H2···N2^{iii}	0.82	2.05	2.730(4)	141
O3–H3···O2^{iv}	0.82	1.86	2.637(4)	158
N3–H3N···O3^{iv}	0.86	2.04	2.884(4)	167
Complex II				
O2–H2···N2^{v}	0.82	2.30	2.748(6)	115
O3–H3···O2^{iv}	0.82	1.89	2.661(6)	157
N3–H3N···O3^{iv}	0.86	2.05	2.897(5)	170

Symmetry codes: ^{i} $-x, -y+1, -z$; ^{ii} $x-2, y+1, z$; ^{iii} $x, -y+1/2, z-1/2$; ^{iv} $-x+1, -y, -z+1$; ^{v} $x, -y+1/2, z+1/2$.

2.4. Cytotoxic activity

Cytotoxic activity was determined in MDA-MB-231, THP-1 and HUVEC cell lines.

When we initially evaluated the data on the THP-1 cell line, H_2***L1***, H_2***L2***, H_2***L3***, **Complex I**, **Complex II**, **Complex III** and cisplatin treatments reduced THP-1 cell viability compared to control cells dose-dependently (Fig. S3†). The IC_{50} values of **Complex I**, **Complex II**, **Complex III** and cisplatin tested in the THP-1 cell line are given as 3.39 ± 0.17 μM, 6.12 ± 0.22 μM, 14.9 ± 2.7 μM and 5.4 ± 1.7 μM, respectively, as shown in Table 4. In THP-1 cells, **Complex III** showed less cytotoxic effect in reducing viability than the others. It was determined that the ligand (**H_2*L3***) of this complex did not effectively reduce viability and its IC_{50} value was above 50 μM.

Based on the results, it was determined that **Complex I** showed more cytotoxic effects than **Complex II**, **Complex III** and cisplatin on the THP-1 cell line. The fact that the ligands and the complexes reduced cell viability at the same rate in THP-1 cells suggests that the cellular effect may be a ligand-based effect.

When the changes obtained with H_2***L1***, H_2***L2***, H_2***L3***, **Complex I**, **Complex II**, **Complex III**, and cisplatin treatments were evaluated, the viability of MDA-MB-231 cells was dose-dependently reduced compared to that of control cells (Fig. S4†). According to the IC_{50} values given in Table 4, the IC_{50} value of **Complex I** was determined as 14.7 ± 0.32. The IC_{50} value of **Complex II** was determined as 13 ± 1.2 μM and that of cisplatin was 7.67 ± 0.32 μM. In this case, the cytotoxic effect of **Complex I** in MDA-MB-231 cells occurred at a concentration 2 times higher than that in cisplatin treatment. Additionally, **Complex III** also reduced viability dose-dependently, and the IC_{50} value was 16 ± 1.3 μM (Table 4).

Table 4 IC_{50} values of compounds tested in cell lines (IC_{50} values were calculated according to MTT test analysis with the GraphPad Prism program in THP-1, MDA-MB-231, and HUVEC cell lines. The table was produced using 50 μM as the cut-off value.)

Cell lines	Compounds	IC_{50} values[a] (μM)
THP-1	**Complex I**	3.39 ± 0.17
	Complex II	6.12 ± 0.22
	Complex III	14.9 ± 2.7
	Cisplatin	**5.4 ± 1.7**
	H_2L1	3.92 ± 0.13
	H_2L2	9.02 ± 1.3
	H_2L3	>50
MDA	**Complex I**	14.7 ± 0.32
	Complex II	13 ± 1.2
	Complex III	16 ± 1.3
	Cisplatin	**7.67 ± 0.32**
	H_2L1	27.7 ± 0.1
	H_2L2	25.8 ± 1.5
	H_2L3	>50
HUVEC	**Complex I**	10.9 ± 0.42
	Complex II	14.6 ± 0.95
	Complex III	27.7 ± 2.6
	Cisplatin	**3.85 ± 0.22**
	H_2L1	>50
	H_2L2	>50
	H_2L3	>50

[a] IC_{50}: these values represent the concentration required to inhibit 50% of cell growth compared to the untreated control cell group. The results are given as the mean ± SEM (standard error of mean).

The IC_{50} values obtained in MDA-MB-231 cells were higher than those in THP-1 cells, which can be attributed to the greater resistance of MDA-MB-231 cells. Numerous genetic differences exist between the two cell lines. Considering these results, when the cell lines are evaluated in terms of p53, which plays a critical role in cellular processes, the TP53 gene status in THP-1 and MDA-MB-231 cells reveals distinct, significant genetic mutations. THP-1 cells, derived from acute monocytic leukemia, exhibit a deletion-frameshift TP53 mutation, resulting in a truncated p53 protein that affects its role in cell cycle regulation and apoptosis.[49–51] In contrast, MDA-MB-231 cells, originating from triple-negative breast cancer, harbor an R280K mutation in the TP53 gene, resulting in dysfunctional p53 activity and a loss of its tumor-suppressive function. This mutation confers resistance to apoptosis and supports the aggressive, metastatic characteristics of MDA-MB-231 cells.[52] Additionally, MYC and BCL2 oncogenes, known to play a role in cell proliferation and apoptosis inhibition, have been reported to be overexpressed in THP-1 cells.[53] Several genes associated with aggressiveness, including KRAS, BRAF, VEGF, and MMPs, further promote proliferative and metastatic properties in MDA-MB-231 cells compared to the THP-1 cell line.[54–56]

The effect of ligands in the HUVEC cell line was not dose-dependent, but **Complex I**, **Complex II**, **Complex III**, and cisplatin treatments dose-dependently reduced cell viability compared with that in control cells. As an important finding, the complexes showed less cytotoxicity than the cytotoxic effect of cisplatin on healthy cells (Fig. S5†). The IC_{50} value of cisplatin in the HUVEC cell line is 3.85 ± 0.22 μM, while **Complex I** and **Complex II** are 10.9 ± 0.42 μM and 14.6 ± 0.95 μM, respectively. Besides, **Complex III** had a slight cytotoxic effect in HUVEC cells (27.7 ± 2.6 μM) (Table 4). The microscope images (20×) of all cell lines treated with **Control**, **H_2L1**, **H_2L2**, **H_2L3**, **Complex I**, **Complex II**, **Complex III**, and **cisplatin** are presented in Fig. S6 in the ESI† and only control, **H_2L1** and **Complex I** among them are shown in Fig. 5.

As a result, it is important that these new synthesized compounds kill cancerous cells at lower concentrations while having fewer side effects on healthy cells.

In a study, it was reported that the Cu(II) complex synthesized, which is similar in structure, had an IC_{50} value of over 20 μM in MDA-MB-231 cells.[57] However, the IC_{50} value of the Ni(II) complex synthesized in our study was below 20 μM and was determined as 14.7 ± 0.32 μM. In connection with these data, it was determined that **Complex I** was effective at lower concentrations on the same cell line. Nickel can form functionally rich molecular geometries, enabling the formation of complexes with advanced properties. This contributes to improving drug properties without any increase in cellular drug resistance or adverse side effects of drugs.[58] Moreover, it is a remarkable result that the Ni(II) complexes exhibit less cytotoxic effect than cisplatin on the HUVEC cell line, which was used as the healthy control cell in our study. Another interesting result was that not only the complexes but also the ligands had cytotoxic effects on the THP-1 cell line.

However, cytotoxicity analyses are considered the beginning of understanding whether a molecule is toxic to humans or its effect on the viability of cancer cells, but they are still not sufficient to understand oral bioavailability. Before moving on to much more expensive research, many scientists have been trying to create drug similarity criteria for many years by using the physical or structural properties of drug molecules.[59] Lipinski *et al.* stated four rules for the effectiveness of a molecule as an oral drug in 1997; in general, there are four criteria and the cutoffs for each of the four parameters are all close to 5 or a multiple of 5. These are related to lipophilicity (C log *P*), molecular mass,[60] and the number of donors and acceptors for hydrogen bonding.[61] In the following years, new criteria were established, such as molecular flexibility for membrane permeation by Navia,[62] rotatable bonds and a number of H-bond donors and acceptors (or polar surface area) by Veber *et al.* for good oral bioavailability.[63]

2.5. Stability studies

The stabilities of biologically active compounds, **complex I** and **H2*L1***, under pseudo-physiological conditions, were investigated in PBS and DMSO using UV-Vis spectroscopy.[64] When performing the stability test in PBS, DMF was used instead of DMSO due to the possibility of forming adduct complexes with DMSO (2% DMF as a solubilizer, 40 μM compound concentration, and pH 7.4). The absorbance spectra were collected after 0, 1, 3, 6, 12 and 24 h. In addition, the behaviour of

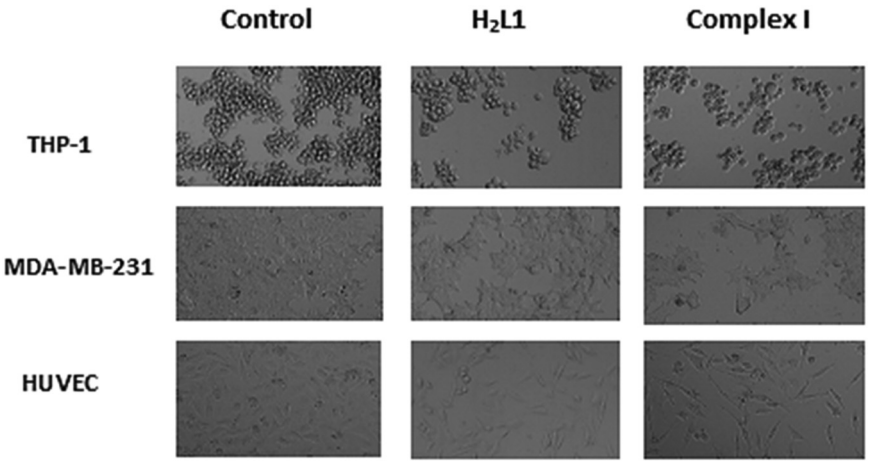

Fig. 5 Representative microscopy images (20×) of all cell lines treated with H_2***L1*** and **Complex I** at their IC_{50} concentrations for 72 hours, compared to the **Control** (the others are presented in the ESI†).

Complex I and **H2*L1*** with pH changes (pH 7.0, pH 7.2, pH 7.4, pH 7.6 and pH 7.8) was investigated (Fig. S7–S14†).

3. Experimental

3.1. Chemicals and apparatus

All chemicals were used as commercially purchased without further purification at reagent grade. The solvents used were HPLC pure. Elemental analyses of all the compounds were performed on a Thermo Finnigan Flash EA 1112 Series. IR spectra of the compounds were recorded on a Cary 630 FTIR spectrometer with a diamond ATR from Agilent in the 4000–400 cm^{-1} range. The electronic spectra of the compounds were recorded on a Shimadzu UV-2600 model UV-Vis spectrophotometer in the 200–800 nm range using 5×10^{-5} M solutions in $CHCl_3$. The ^{1}H-NMR spectra of the compounds were recorded on a Varian UNITY INOVA 500 MHz NMR spectrometer using deuterated DMSO as solvent at 25 ± 2 °C. Single-crystal X-ray diffraction studies were carried out using an STOE IPDS II diffractometer at room temperature.

3.2. Synthesis of the compounds

Synthesis of the ligands (H_2*L1*, H_2*L2* and H_2*L3*). 3,5-Dihalogenosalicylaldehyde-*S*-methyl-isothiosemicarbazone ligands were obtained according to a literature method.[65] An equimolar quantity of *S*-methyl isothiosemicarbazide (1 g) and 3,5-di-X, X-substituted salicylaldehyde (X: Cl for ***L1*** (1.91 g), X: Br for ***L2*** (2,8 g), X: I ***L3*** (3.74)) were refluxed for 2 h and the products were filtered. The resulting yellow products were dried under vacuum and recrystallized in DCM : hexane (v/v = 1/2) solution.

H_2*L1*. Color: yellow; yield: 94%; m.p. (°C): 194–195; Anal. Calc.% (found %) for $C_9H_9N_3Cl_2OS$ (278.16 g) C, 38.65 (38.86); H, 3.21 (3.20); N, 14.27 (14.58); S, 11.68 (11.53). IR (ATR, cm^{-1}): 3481 ν(OH); 3278 $\nu_{sym}(NH_2)$; 3240 $\nu_{asym}(NH_2)$; 3077, 2957, 2925 ν(C–H); 1628 δ(N–H); 1609, 1576 ν(C=N); 1152 ν(C–O); 734 ν(C–S). UV-Vis (λ, nm (ε)) 218.5 (8700), 240.50 (19 700), 302 (23 600), 316 (22 300), 345 (18 400). ^{1}H-NMR (ppm): 12.59, 11.81 (*cis*/*trans* ratio: 3/1, s, 1H, OH), 8.45, 8.35 (*syn*/*anti* ratio: 1/3, s, 1H, CH=N^1), 7.54 (d, 1H, J = 2,45, *d*), 7.51 (d, J = 2.44, 1H, *b*), 7.20 (s, broad, 2H, NH_2), 2.47, 2.39 (*cis*/*trans* ratio: 1/2, s, 3H, S-CH_3).

H_2*L2*. Color: yellow; yield: 92%; m.p. (°C): 199; Anal. Calc.% (found %) For $C_9H_9N_3Br_2OS$ (367.06 g) C, 29.69 (29.65); H, 2.49 (2.47); N, 11.25 (11.20); S, 8.24 (8.33). IR (ATR, cm^{-1}): 3467 ν(OH); 3281 $\nu_{sym}(NH_2)$; 3239 $\nu_{asym}(NH_2)$; 3060, 2981, 2923 ν(C–H); 1653 δ(N–H); 1629, 1595 ν(C=N); 1147 ν(C–O); 734 ν(C–S). UV-Vis (λ, nm (ε)) 211.5 (8400), 224.50 (9200), 237.50 (16 400), 305 (18 320), 346 (15 600). ^{1}H-NMR (ppm): 12.58, 10.76 (*cis*/*trans* ratio: 4/1, s, 1H, OH), 8.56, 8.35 (*syn*/*anti* ratio: 1, s, 1H, CH=N^1), 8.15, 7.35 (*cis*/*trans* ratio: 1, s, broad, 2H, NH_2), 7.87 (m, 1H, *d*), 7.71 (d, J = 2.15, 1H, *b*), 2.66, 2.48 (*cis*/*trans* ratio: 1/2, s, 3H, S-CH_3).

H_2*L3*. Color: yellow; yield: 89%; m.p. (°C): 169; Anal. Calc.% (found %) For $C_9H_9N_3I_2OS$ (461.06 g) C, 23.45 (23.50); H, 1.97 (1.95); N, 9.11 (9.13); S, 6.95 (6.92). IR (ATR, cm^{-1}): 3460 ν(OH); 3244 $\nu_{sym}(NH_2)$; 3153 $\nu_{asym}(NH_2)$; 3043, 3009, 2925 ν(C–H); 1653 δ(N–H); 1619, 1593 ν(C=N); 1155 ν(C–O); 734 ν(C–S). UV-Vis (λ, nm (ε)) 208 (8400), 238 (25 480), 308.50 (19 620), 320.50 (18 900), 350.50(14 560). ^{1}H-NMR (ppm): 12.79, 12.19 (*cis*/*trans* ratio: 4/1, s, 1H, OH), 9.88, 8.24 (*syn*/*anti* ratio: 1/2, s, 1H, CH=N^1), 8.34, 7.18 (*cis*/*trans* ratio:1, s, broad, 2H, NH_2), 7.94 (d, J = 2.00, 1H, *d*), 7.79 (d, J = 2.05, 1H, *b*), 2.45, 2.37 (*cis*/*trans* ratio: 1/2, s, 3H, S-CH_3).

Synthesis of the complexes. For **Complex I**, $NiCl_2{\cdot}6H_2O$ (0.24 g, 1 mmol) was added to the methanolic solution of H_2***L1*** (0.28 g, 1 mmol) at 60 °C. The obtained solution was refluxed for 1 h, and then diethanolamine was added to the reaction medium. The resulting bright red solution was refluxed for 3 hours. After 2 weeks, red crystals were filtered and dried under vacuum.

Complex II and **Complex III** were synthesized using a similar method to **Complex I** by using 3,5-dibromosalicylalde-

hyde-*S*-methyl-isothiosemicarbazone (**H_2L2**) and 3,5-diiodosalicylaldehyde-*S*-methyl-isothiosemicarbazone (**H_2L3**) instead of 3,5-dichlorosalicylaldehyde-*S*-methyl-isothiosemicarbazone. A red powder product was obtained for both complexes and filtered. The products were recrystallized in DCM : methanol (v/v: 1/2) solution.

Complex I. Color: red; yield: 74%; m.p. (°C): 339; Anal. Calc. % (found %) for $C_{13}H_{18}N_4Cl_2O_3SNi$ (439.98 g) C, 35.56 (35.49); H, 4.11 (4.12); N, 12.66 (12.73); S, 7.31 (7.29). IR (ATR, cm^{-1}): 3481 ν(OH); 3278 $\nu(N^4H)$; 3244 $\nu(NH_{dea})$; 3082, 2957, 2923 $\nu(C\text{-}H_{DEA})$; 1624 δ(N–H); 1585, 1560 ν(C=N); 1179 ν(C–O); 731 ν(C–S). UV-Vis (λ, nm (ε)) 214.50 (9880), 241 (23 900), 300.50 (6740), 374.50 (14 580). ^{1}H-NMR (ppm): 8.00 (s, 1H, $CH{=}N^1$), 7.46 (d, J = 2.44, 1H, *d*), 7.32 (t, J = 2.44, 1H, *b*), 4.99 (t, J = 4.64, 2H, *x*, *x*), 4.49 (s, broad, 2H, *x*, *x*), 4.46 (d, J = 0.49, 2H, *y*, *y*), 4.28 (t, 2H, J = 1.35, J = 1.96, *y*, *y*), 2.95 (s, broad, 1H, OH), 2.40 (s, broad, 1H, OH), 2.39 (s, broad, NH), 2.37 (s, 3H, S-CH_3).

Complex II. Color: bright red; yield: 72%; m.p. (°C): 245; Anal. Calc.% (found %) for $C_{13}H_{18}N_4Br_2O_3SNi$ (528.87 g) C, 29.56 (29.52); H, 3.21 (3.28) N, 10.76 (10.59); S, 8.24 (8.29). IR (ATR, cm^{-1}): 3370 ν(OH); 3290 $\nu(N^4H)$; 3271 $\nu(NH_{DEA})$; 2926, 2901, 2864 $\nu(C\text{–}H_{DEA})$; 1654, 1636 δ(N–H); 1596, 1577 ν(C=N); 1150 ν(C–O); 731 ν(C–S). UV-Vis (λ, nm (ε)) 214.50 (8800), 243 (21 080), 312.50 (5580), 384 (11 640). ^{1}H-NMR (ppm): 7.99 (s, 1H, $CH{=}N^1$), 7.62 (d, J = 2.44, 1H, *d*), 7.55 (d, J = 2.44, 1H, *b*), 4.99 (t, J = 4.79, 2H, *x*, *x*), 4.50 (s, broad, 2H, *x*, *x*), 4.48 (m, 2H, *y*, *y*), 4.29 (m, 2H, *y*, *y*), 3.85 (s, broad, 1H, OH), 3.00 (s, broad, 1H, OH), 2.40 (s, broad, 1H, NH), 2.39 (s, broad, 1H, NH), 2.37 (s, 3H, S-CH_3).

Complex III. Color: red; yield: 71%; m.p. (°C): 270 (decomposition); Anal. Calc.% (found %) for $C_{13}H_{18}N_4I_2O_3SNi$ (622.87 g) C, 25.07 (25.06); H, 2.91 (2.94) N, 8.99 (8.97); S, 5.15 (5.13). IR (ATR, cm^{-1}): 3419 ν(OH); 3321 $\nu(N^4H)$; 3211 $\nu(NH_{DEA})$; 2983, 2924, 2886 $\nu(C\text{–}H_{DEA})$; 1653, 1636 δ(N–H); 1613, 1597 ν(C=N); 1151 ν(C–O); 781 ν(C–S). UV-Vis (λ, nm (ε)) 204.50 (7000), 240 (17 120), 311 (4540), 382.50 (9400). ^{1}H-NMR (ppm): 7.91 (s, 1H, $CH{=}N^1$), 7.54 (d, J = 2.44, 1H, *d*), 7.12 (dd, J = 8.79, J = 2.44, 1H, *b*), 4.92 (t, J = 4.64, J = 4.64, 2H, *x*, *x*), 4.42 (s, broad, 2H, *x*, *x*), 4.31 (s, broad, 2H, *y*, *y*), 4.26 (m, 2H, *y*, *y*), 3.52 (s, broad, 1H, OH), 3.00 (s, broad, 1H, OH), 2.86 (s, broad, NH), 2.40 (s, broad, 1H, NH), 2.39 (s, broad, 1H, NH), 2.37 (s, 3H, S-CH_3).

3.3. X-ray crystallography

Single crystal X-ray diffraction data of the compounds were collected on an STOE IPDS II diffractometer at room temperature using graphite-monochromated Mo Kα radiation by applying the ω-scan method. Data collection and cell refinement were carried out using X-AREA, data reduction was applied using X-RED32.[66] The structures were solved with a dual-space algorithm using SHELXT-2018 [67] and refined by means of the full-matrix least-squares calculations on F^2 using SHELXL-2019.[68] All H atoms were located from different maps and included in the refinements as riding atoms. Crystal data, data collection and structure refinement details are provided in Table 1. Molecular graphics were prepared by using OLEX2.[69]

3.4. Cytotoxicity assay

The MDA-MB-231 human breast cancer cell line, THP-1 human acute monocytic leukaemia cell line and HUVEC human umbilical vein endothelial cell line were obtained from the American Type Culture Collection (ATCC) (VA, U.S.A.). Cisplatin, an antineoplastic drug, was purchased from Koçak Farma. Cells were cultured according to the standard procedure and maintained in Dulbecco's modified Eagle's medium (DMEM, Sigma, Chemical Co., St Louis, MO) and RPMI-1640 (Sigma, Chemical Co., St Louis, MO) medium. Medium solutions were supplemented with 10% FBS and 1% penicillin/streptomycin. The cells were cultured in a standard humidified incubator at 5% CO_2 at 37 °C. The number of viable cells was calculated using the trypan blue dye exclusion test. Cells were grown in 96-multiwell flat bottom microtiter plates with 10 000 cells/100 μL of complete medium per well. Ligands and complexes were prepared as stock solutions (5 mg mL^{-1}, DMSO). Then, dilutions of the tested concentrations were obtained using culture medium. Concentrations were in the range of 1–50 μM per well. 10 μl was added to wells, each one in triplicate. DMSO was added to the control wells at 0.1%. After plating THP-1, MDA-MB-231 and HUVEC cells, they were cultured for three days in the incubator. The cytotoxic activity of complexes and ligands was evaluated using MTT (3-(4,5-dimethylthiazol-2-yl)-2,5-diphenyl-2*H*-tetrazolium-bromide) assay.[70] The plates were incubated for 72 hours, and evaluation of cell viability was performed by using the MTT colorimetric assay. 10 μL MTT solution (5 mg mL^{-1} in PBS, Sigma) was added to each well and incubated for 3.5 hours at 37 °C. Then, formazan crystals were solubilized in 100 μL DMSO. Optical density was measured by using a Rayto microplate reader at 560 nm with a reference wavelength of 620 nm. In each experiment, 5 different concentrations were analyzed with 3 replicate microplate wells for each concentration. Since each test is repeated 3 times, the cytotoxicity of each concentration was evaluated with 9 individual cell cultures. According to the absorbance values obtained, the IC_{50} values of all compounds tested in the cell lines were calculated using GraphPad Prism 9 software. Statistical analyses were performed nonparametrically with Student's t-test, and the results were compared to those of the control.

3.5. Stability studies

The stabilities of biologically active compounds, **complex I** and **H2*L1***, under pseudo-physiological conditions were determined in PBS for 24 h using UV-Vis spectroscopy (2% DMF as a solubilizer, 40 μM compound concentration, and pH 7.4). The behaviours of **complex I** and **H2*L1*** with the pH changes (pH 7.0, pH 7.2, pH 7.4, pH 7.6 and pH 7.8) were also investigated. The compounds were in a neutral form at pH 7.4 (physiological pH), and no turbidity or aggregation was observed with the addition of buffer, even after 24 hours in solution. In addition, no significant change was observed in the UV spectra, except for a slight decrease in absorbance over time.

4. Conclusion

The mixed ligand nickel(II) complexes from the 3,5-dihalogeno-salicylaldehyde-*S*-methylisothiosemicarbazone (halogen: Cl, Br, I) ligands and diethanolamine were synthesized, and their structures were determined by single crystal X-ray diffraction. Their cytotoxic activities were investigated on MDA-MB-231, THP-1, and HUVEC cell lines.

The crystal structure of the ligand is in a square planar geometry with intramolecular and intermolecular hydrogen bonding. On complexation, the *Z* conformation of the ligand changes to the *E* conformer by rotation around the N2═C8 bond upon coordination with the metal. In the complexes, Ni atoms are in a distorted square geometry, surrounded by the N atom of diethanolamine and by the O (phenolic), N1 (imine), and N3 (amine) atoms of thiosemicarbazone. While intramolecular interactions are not seen in the molecular structure of the complexes, intermolecular interactions are the same in both complexes. The complexes showed supramolecular characteristics. Another difference is that the halogen atoms are free in the molecule without participating in any interaction in the crystal structure of the complex.

According to Lipinski's rule of five, a compound to evaluate orally active drugs in humans has no more than 5 hydrogen bond donors (sum of NHs and OHs) and no more than 10 hydrogen bond acceptors (sum of Ns and Os). In this study, ligands have three hydrogen donor atoms and four acceptor atoms for hydrogen bonding. The **H_2L1** ligand has in total five H-bonds including intra-, inter-molecular, and X···H hydrogen bonds in the crystal structure, whereas**Complexes I** and **II** have three hydrogen donor and four acceptor atoms, forming six H-bonds in total. Therefore, the ligands and complexes obeyed both of Lipinski's mentioned rules.

In the other two rules of Lipinski, the candidate drug has a molecular mass of less than 500 Da and a partition coefficient not greater than 5 (or MLog *P* is under 4.15). In this study, molecular masses of the synthesized ligands, **H_2L1**, **H_2L2** and **H_2L3**, are 278.16, 367.06 and 461.06 g mol^{-1}, respectively, while those of the complexes **Complex I**, **Complex II**, and **Complex III** are 439.98, 528.87 and 622.87 mol g^{-1}. The MiLog *P* values of **H_2L1**, **H_2L2** and **H_2L3** are calculated as 2.59, 2.85 and 3.40, respectively.[71]

On the other hand, Veber proposed the best approach for oral absorption potential by passive processes where the number of rotatable bonds should be 10 or fewer, and the number of H-bond donors and acceptors should be ≤12 (or a value of polar surface area (PSA) equal to or less than 140 $Å^2$). In our study, the number of rotatable bonds on the ligands and complexes are 2 and 5, respectively, and the numbers of H bond donors and acceptors are fewer than 12. In that case, the values of ligands and complexes obeyed Veber's mentioned rules.

The cytotoxicity assays of the ligands and complexes were performed on cancer cell lines (THP-1 and MDA-MB-231) and a healthy cell line (HUVEC). The rank order for cytotoxicity of the compounds on THP-1 cells was **Complex I** > **H_2L1** > **cisplatin** > **Complex II** > **H_2L2** > **Complex III** > **H_2L3**. The 3,5-dichloro-substituted thiosemicarbazone ligand (IC_{50}: 3.39 ± 0.17 μM) and its complex (IC_{50}: 3.92 ± 0.13 μM) are more cytotoxic than those of cisplatin (IC_{50}: 5.4 ± 1.7 μM) and other ligands and complexes. It was observed that the cytotoxicity of the compounds on MDA-MB-231 cells was not as effective as on THP-1 cells, and cisplatin was more toxic than others. The most effective compounds in MDA-MB-231 cells were **Complex I** (14.7 ± 0.32 μM) and **Complex II** (13 ± 1.2 μM), which had relatively high IC_{50} values.

The cytotoxicity results on the HUVEC healthy cell line showed that cisplatin was the most toxic, with a 3.85 ± 0.22 μM value, lower than those of **Complex I** (10.9 ± 0.42 μM), **Complex II** (14.6 ± 0.95 μM), and **Complex III** (27.7 ± 2.6 μM), whereas the least toxic compounds were ligands with higher values than 50 μM.

As the ligands and complexes move from chlorine to iodine, the decrease in cytotoxicity parallels the decrease in electronegativity and increase in the diameter of the halogen atom. Chloro-substituted derivatives were noted to be the most active compounds.

As a result, taking into account the cytotoxicity value and performance of drug-likeness criteria, **H_2L1** and **Complex I** can be considered as candidate compounds for further investigation in terms of their therapeutic properties in THP-1 cancer cells.

Data availability

The authors declare that the data supporting the findings of this study are available within the paper and its ESI files.†

CCDC 2288067–2288069 contain the supplementary crystallographic data for the compounds reported in this article.†

Conflicts of interest

There are no conflicts to declare.

Acknowledgements

This work was supported by the Scientific Research Projects Coordination Unit of Istanbul University-Cerrahpaşa (Project numbers: FYO-2021-35061 and FDK-2021-35467) and The Scientific and Technological Research Council of Turkiye (TUBITAK Project number: 222Z290).

References

1 L. Kelland, The resurgence of platinum-based cancer chemotherapy, *Nat. Rev. Cancer*, 2007, 7, 573–584, DOI: 10.1038/nrc2167.

2 L. Galluzzi, L. Senovilla, I. Vitale, J. Michels, I. Martins, O. Kepp, M. Castedo and G. Kroemer, Molecular mecha-

nisms of cisplatin resistance, *Oncogene*, 2012, **31**, 1869–1883, DOI: 10.1038/onc.2011.384.

3 S. N. Aleksakhina, A. Kashyap and E. N. Imyanitov, Mechanisms of acquired tumor drug resistance, *Biochim. Biophys. Acta, Rev. Cancer*, 2019, **1872**, 188310, DOI: 10.1016/j.bbcan.2019.188310.

4 Y. Sun, Y. Lu, M. Bian, Z. Yang, X. Ma and W. Liu, Pt(II) and Au(III) complexes containing Schiff-base ligands: A promising source for antitumor treatment, *Eur. J. Med. Chem.*, 2021, **211**, 113098, DOI: 10.1016/j.ejmech.2020.113098.

5 B. Mansoori, A. Mohammadi, S. Davudian, S. Shirjang and B. Baradaran, The different mechanisms of cancer drug resistance: A brief review, *Adv. Pharm. Bull.*, 2017, **7**, 339–348, DOI: 10.1016/10.15171/apb.2017.041.

6 A. L. Lainé and C. Passirani, Novel metal-based anticancer drugs: A new challenge in drug delivery, *Curr. Opin. Pharmacol.*, 2012, **12**, 420–426, DOI: 10.1016/10.1016/j.coph.2012.04.006.

7 M. A. Arafath, F. Adam, M. B. K. Ahamed, M. R. Karim, M. N. Uddin, B. M. Yamin and A. Abdou, Ni(II), Pd(II) and Pt(II) complexes with SNO-group thiosemicarbazone and DMSO: Synthesis, characterization, DFT, molecular docking and cytotoxicity, *J. Mol. Struct.*, 2023, **1278**, 134887, DOI: 10.1016/j.molstruc.2022.134887.

8 O. Ertik, S. Tunali, E. T. Acar, T. Bal-Demirci, B. Ülküseven and R. Yanardağ, Antioxidant Activity and Protective Effects of an Oxovanadium(IV) Complex on Heart and Aorta Injury of STZ-Diabetic Rats, *Biol. Trace Elem. Res.*, 2024, **202**, 2085–2099, DOI: 10.1007/s12011-023-03802-0.

9 E. Avcu Altiparmak, S. Yazar, N. Özdemir, T. Bal-Demirci and B. Ülküseven, Supramolecular Ni(II) complex aggregates with a circular linkage of intermolecular multi-hydrogen bonding frameworks based on thiosemicarbazone, and a Cu(II) complex: Synthesis, structural, DFT, electrochemical and antioxidant studies, *Polyhedron*, 2021, **209**, 115457, DOI: 10.1016/j.poly.2021.115457.

10 A. Karaküçük-Iyidoğan, D. Taşdemir, E. E. Oruç-Emre and J. Balzarini, Novel platinum(II) and palladium(II) complexes of thiosemicarbazones derived from 5-substitutedthiophene-2-carboxaldehydes and their antiviral and cytotoxic activities, *Eur. J. Med. Chem.*, 2011, **46**, 5616–5624, DOI: 10.1016/j.ejmech.2011.09.031.

11 N. C. Kasuga, K. Onodera, S. Nakano, K. Hayashi and K. Nomiya, Syntheses, crystal structures and antimicrobial activities of 6-coordinate antimony(III) complexes with tridentate 2-acetylpyridine thiosemicarbazone, bis(thiosemicarbazone) and semicarbazone ligands, *J. Inorg. Biochem.*, 2006, **100**, 1176–1186, DOI: 10.1016/j.jinorgbio.2006.01.037.

12 T. Bal-Demirci, Ş. Güveli, S. Yeşilyurt, N. Özdemir and B. Ülküseven, Thiosemicarbazone ligand, nickel(II) and ruthenium(II) complexes based on vitamin B6 vitamer: The synthesis, different coordination behaviors and antioxidant activities, *Inorg. Chim. Acta*, 2020, **502**, 119335, DOI: 10.1016/j.ica.2019.119335.

13 R. Yanardag, T. B. Demirci, B. Ülküseven, S. Bolkent, S. Tunalı and S. Bolkent, Synthesis, characterization and antidiabetic properties of N1-2,4-dihydroxybenzylidene-N4–2-hydroxybenzylidene-S-methyl-thiosemicarbazidato-oxovanadium(IV), *Eur. J. Med. Chem.*, 2009, **44**, 818–826, DOI: 10.1016/j.ejmech.2008.04.023.

14 B. Atasever, B. Ülküseven, T. Bal-Demirci, S. Erdem-Kuruca and Z. Solakoğlu, Cytotoxic activities of new iron(III) and nickel(II) chelates of some S-methyl-thiosemicarbazones on K562 and ECV304 cells, *Invest. New Drugs*, 2010, **28**, 421–432, DOI: 10.1007/s10637-009-9272-2.

15 E. Avcu Altiparmak, G. Erdemir, N. Özdemir, S. E. Kuruca and T. Bal-Demirci, Cu(ii) salen and 1,2,4-triazole complexes from thiosemicarbazone: Synthesis, physicochemical and structural properties and cytotoxic activities, *New J. Chem.*, 2020, **44**, 5333–5342, DOI: 10.1039/c9nj04455h.

16 F. D. Kalındemirtaş, B. Kaya, M. Bener, O. Şahin, S. E. Kuruca, T. B. Demirci and B. Ülküseven, Iron(III) complexes based on tetradentate thiosemicarbazones: Synthesis, characterization, radical scavenging activity and in vitro cytotoxicity on K562, P3HR1 and JURKAT cells, *Appl. Organomet. Chem.*, 2021, **35**, e6157, DOI: 10.1002/aoc.6157.

17 T. Bal-Demirci, M. Şahin, E. KondakÒ«i, M. Özyürek, B. Ülküseven and R. Apak, Synthesis and antioxidant activities of transition metal complexes based 3-hydroxysalicylaldehyde-S-methylthiosemicarbazone, *Spectrochim. Acta, Part A*, 2015, **138**, 866–872, DOI: 10.1016/j.saa.2014.10.088.

18 D. Özerkan, O. Ertik, B. Kaya, S. E. Kuruca, R. Yanardağ and B. Ülküseven, Novel palladium(II) complexes with tetradentate thiosemicarbazones: Synthesis, characterization, in vitro cytotoxicity and xanthine oxidase inhibition, *Invest. New Drugs*, 2019, **37**, 1187–1197, DOI: 10.1007/s10637-019-00763-8.

19 F. Danışman-Kalındemirtaş, S. Erdem-Kuruca, G. E. Cilasun, E. Sert, D. Özerkan, T. B. Demirci, B. Ülküseven and İ. A Kariper, Enhanced anticancer effect of newly synthesised albumin-bound Fe(III)-S-methyl-thiosemicarbazones on breast cancer cells, *J. Taibah. Univ. Sci.*, 2023, **17**(1), 2375454, DOI: 10.1080/16583655.2023.2375454.

20 P. J. Jansson, P. C. Sharpe, P. V. Bernhardt and D. R. Richardson, Novel thiosemicarbazones of the ApT and DpT series and their copper complexes: Identification of pronounced redox activity and characterization of their antitumor activity, *J. Med. Chem.*, 2010, **53**, 5759–5769, DOI: 10.1021/jm100561b.

21 A. Kotian, V. Kamat, K. Naik, D. Kokare, K. Kumara, K. Neratur, V. Kumbar, K. Bhat and V. Revankar, 8-Hydroxyquinoline derived p-halo N4-phenyl substituted thiosemicarbazones: Crystal structures, spectral characterization and in vitro cytotoxic studies of their Co(III), Ni(II) and Cu(II) complexes, *Bioorg. Chem.*, 2021, **112**, 104962, DOI: 10.1016/j.bioorg.2021.104962.

22 N. E. Dixon, C. Gazzola, J. J. Watters, R. L. Blakeley and B. Zerner, Jack Bean Urease (EC 3.5.1.5) A metalloenzyme. A simple biological role for nickel, *J. Am. Chem. Soc.*, 1975, **97**, 4131–4133.

23 B. Zambelli, F. Musiani, S. Benini and S. Ciurli, Chemistry of Ni2 + in urease: Sensing, trafficking, and catalysis, *Acc. Chem. Res.*, 2011, **44**, 520–530, DOI: 10.1021/ar200041k.

24 P. P. Netalkar, S. P. Netalkar and V. K. Revankar, Transition metal complexes of thiosemicarbazone: Synthesis, structures and invitro antimicrobial studies, *Polyhedron*, 2015, **100**, 215–222, DOI: 10.1016/j.poly.2015.07.075.

25 S. Chandra, S. Parmar and Y. Kumar, Synthesis, spectroscopic, and antimicrobial studies on bivalent zinc and mercury complexes of 2-formylpyridine thiosemicarbazone, *Bioinorg. Chem. Appl.*, 2009, **2009**, 851316, DOI: 10.1155/2009/851316.

26 S. Savir, Z. J. Wei, J. W. K. Liew, I. Vythilingam, Y. A. L. Lim, H. M. Saaf, K. S. Sim and K. W. Tan, Synthesis, cytotoxicity and antimalarial activities of thiosemicarbazones and their nickel(II) complexes, *J. Mol. Struct.*, 2020, **1211**, 128090, DOI: 10.1016/j.molstruc.2020.128090.

27 M. Carcelli, S. Montalbano, D. Rogolino, V. Gandin, F. Miglioli, G. Pelosi and A. Buschini, Antiproliferative activity of nickel(II), palladium(II) and zinc(II) thiosemicarbazone complexes, *Inorg. Chim. Acta*, 2022, **533**, 120779, DOI: 10.1016/j.ica.2021.120779.

28 G. Kalaiarasi, C. Umadevi, A. Shanmugapriya, P. Kalaivani, F. Dallemer and R. Prabhakaran, DNA(CT), protein(BSA) binding studies, anti-oxidant and cytotoxicity studies of new binuclear Ni(II) complexes containing 4(N)-substituted thiosemicarbazones, *Inorg. Chim. Acta*, 2016, **453**, 547–558, DOI: 10.1016/j.ica.2016.09.006.

29 E. Ramachandran, P. Kalaivani, R. Prabhakaran, N. P. Rath, S. Brinda, P. Poornima, V. V. Padma and K. Natarajan, Synthesis, X-ray crystal structure, DNA binding, antioxidant and cytotoxicity studies of Ni(II) and Pd(II) thiosemicarbazone complexes, *Metallomics*, 2012, **4**, 218–227, DOI: 10.1039/c1mt00143d.

30 M. Jagadeesh, M. Lavanya, S. K. Kalangi, Y. Sarala, C. Ramachandraiah and A. Varada Reddy, Spectroscopic characterization, antioxidant and antitumour studies of novel bromo substituted thiosemicarbazone and its copper(II), nickel(II) and palladium(II) complexes, *Spectrochim. Acta, Part A*, 2015, **135**, 180–184, DOI: 10.1016/j.saa.2014.06.141.

31 E. Avcu Altiparmak, G. Ozen Eroglu, E. Ozcelik, N. Özdemir, S. Erdem Kuruca, N. Arsu, B. Ülküseven and T. Bal-Demirci, The formation of a metallosupramolecular porous helicate through salicylaldehydethiosemicarbazone: Synthesis, Characterization, Cytotoxic activity, DNA binding and DFT calculations, *Appl. Organomet. Chem.*, 2019, **33**, e5023, DOI: 10.1002/aoc.5023.

32 I. Kiliç-Cikla, Ş. Güveli, M. Yavuz, T. Bal-Demirci and B. Ülküseven, 5-Methyl-2-hydroxy-acetophenone-thiosemicarbazone and its nickel(II) complex: Crystallographic, spectroscopic (IR, NMR and UV) and DFT studies, *Polyhedron*, 2016, **105**, 104–114, DOI: 10.1016/j.poly.2015.12.021.

33 E. Pretsch, P. Bühlmann and M. Badertscher, *Structure determination of organic compounds: Tables of spectral data*, Springer, Berlin, Heidelberg, 2009.

34 M. Smith, *March J March's advanced organic chemistry: reactions, mechanisms, and structure*, Wiley-Interscience, 2007.

35 Ş. Güveli, I. Kılıç-Cıkla, B. Ülküseven, M. Yavuz and T. Bal-Demirci, 5-Methyl-2-hydroxy-acetophenone-S-methyl-thiosemicarbazone and its nickel-PPh3 complex. Synthesis, characterization, and DFT calculations, *J. Mol. Struct.*, 2018, **1173**, 366–374, DOI: 10.1016/j.molstruc.2018.06.102.

36 R. Takjoo, S. M. Mashmoul Moghadam, H. Amiri Rudbari and G. Bruno, Synthesis and X-ray crystal structures of some isothiosemicarbazone complexes, *Transition Met. Chem.*, 2019, **44**, 525–534, DOI: 10.1007/s11243-019-00310-w.

37 B. İlhan Ceylan, A. Yilmaz, O. Bölükbaşı, E. Acar, M. Özyürek, Y. Kurt and B. Ülküseven, A square-pyramidal iron(III) complex obtained from 2-hydroxy-benzophenone-S-allyl-thiosemicarbazone: synthesis, characterization, electrochemistry, quantum chemical studies and antioxidant capability, *J. Coord. Chem.*, 2020, **73**, 120–136, DOI: 10.1080/00958972.2020.1715372.

38 Ş. Güveli, N. Özdemir, T. Bal-Demirci, M. Soylu and B. Ülküseven, Hydrogen-bonded and π-stacked nickel(II) thiosemicarbazone complexes: Synthesis, spectral and structural studies, *Transition Met. Chem.*, 2019, **44**, 115–123, DOI: 10.1007/s11243-018-0275-8.

39 M. Ahmadi, A. Fasihizad, B. Machura, R. Kruszynski and T. Barak, New complexes of an unsymmetrical tetradentate isothiosemicarbazone: Structural, spectral and thermogravimetric investigations, and their nanoparticles synthesis, *Polyhedron*, 2014, **81**, 115–122, DOI: 10.1016/j.poly.2014.05.075.

40 M. F. Zaltariov, M. Hammerstad, H. J. Arabshahi, K. Jovanovic, K. Richter, M. Cazacu, S. Shova, M. Balan, N. Andersen, S. Radulovic, J. Reynisson, K. Andersson and V. Arion, New Iminodiacetate-Thiosemicarbazone Hybrids and Their Copper(II) Complexes Are Potential Ribonucleotide Reductase R2 Inhibitors with High Antiproliferative Activity, *Inorg. Chem.*, 2017, **56**, 3532–3549, DOI: 10.1021/acs.inorgchem.6b03178.

41 R. Takjoo, A. Akbari, M. Ahmadi, H. Amiri Rudbari and G. Bruno, Synthesis, spectroscopy, DFT and crystal structure investigations of 3-methoxy-2-hydroxybenzaldehyde S-ethylisothiosemicarbazone and its Ni(II) and Mo(VI) complexes, *Polyhedron*, 2013, **55**, 225–232, DOI: 10.1016/j.poly.2013.02.078.

42 J. Bernstein, R. E. Davis, L. Shimoni and N. L. Chang, Patterns in Hydrogen Bonding: Functionality and Graph Set Analysis in Crystals, *Angew. Chem., Int. Ed. Engl.*, 1995, **34**, 1555–1573, DOI: 10.1002/anie.199515551.

43 G. A. Bogdanovi, A. S. Bird and M. Leovac, Transition metal complexes with thiosemicarbazide-based ligands. XXXIX. [Benzoylacetone 3-methylisothiosemicarbazonato(2-)-O,N1, N4] (pyridine-N)nickel(II), *Acta Crystallogr., Sect. C: Cryst. Struct. Commun.*, 1999, **55**, 1656–1658.

44 R. Takjoo, R. Centore, A. Akbari and M. Ahmadi, Square planar nickel(II) complexes derived from 5-bromo-2- hydroxybenzaldehyde S-ethylisothiosemicarbazone: Preparation,

characterization and structural studies, *Polyhedron*, 2014, **80**, 243–249, DOI: 10.1016/j.poly.2014.04.055.

45 R. Takjoo, P. Ramasami, A. Hashemzadeh, L. Ryhman, H. Rudbari and G. Bruno, An integrated experimental and theoretical investigation of the structural and spectroscopic properties of two nickel(II) isothiosemicarbazone complexes, *J. Coord. Chem.*, 2014, **67**, 1392–1404, DOI: 10.1080/00958972.2014.916796.

46 V. M. Leovac, V. I. Cesljevic, N. V. Gerbeleu, Y. A. Simonov, A. A. Dvorkin and V. B. Arion, Transition metal complexes with the thiosemicarbazide-based ligands. Part 12. Synthesis, structure and template reaction of ammine [2,4-pentane-dione S-methylisothiosemicarbazonato(2-)]nickel (II) dihydrate, *Transition Met. Chem.*, 1993, **18**, 309–311, DOI: 10.1007/BF00207953.

47 L. Yang, D. R. Powell and R. P. Houser, Structural variation in copper(I) complexes with pyridylmethylamide ligands: Structural analysis with a new four-coordinate geometry index, τ4, *J. Chem. Soc., Dalton Trans.*, 2007, 955–964, DOI: 10.1039/b617136b.

48 A. Okuniewski, D. Rosiak, J. Chojnacki and B. Becker, Coordination polymers and molecular structures among complexes of mercury(II) halides with selected 1-benzoylthioureas, *Polyhedron*, 2015, **90**, 47–57, DOI: 10.1016/j.poly.2015.01.035.

49 K. Sugimoto, H. Toyoshima, R. Sakai, K. Miyagawa, K. Hagiwara, F. Ishikawa, F. Takaku, H. Mizoguchi, Y. Yazaki and H. Hirai, Frequent mutations in the p53 gene in human myeloid leukemia cell lines, *Blood*, 1992, **79**(10), 2378–2383.

50 A. Fleischer and A. Rebollo, Induction of p53-independent apoptosis by the BH3-only protein ITM2Bs, *FEBS Lett.*, 2004, **557**(1–3), 283–287, DOI: 10.1016/S0014-5793(03)01497-8.

51 S. Kamihira, C. Terada, D. Sasaki, K. Yanagihara, K. Tsukasaki, H. Hasegawa and Y. Yamada, Aberrant p53 protein expression and function in a panel of hematopoietic cell lines with different p53 mutations, *Eur. J. Haematol.*, 2009, **82**(4), 301–307, DOI: 10.1111/j.1600-0609.2009.01218.x.

52 M. Coan, M. Toso, L. Cesaratto, I. Rigo, S. Borgna, A. Dalla Pietà, L. Zandonà, L. Iuri, A. Zucchetto, C. Piazza, G. Baldassarre, R. Spizzo and M. S. Nicoloso, *LINC01605* is a novel target of mutant p53 in breast and ovarian cancer cell lines, *Int. J. Mol. Sci.*, 2023, **24**(18), 13736, DOI: 10.3390/ijms241813736.

53 Y. Lu, X. Jiang, Y. Li, F. Li, M. Zhao, Y. Lin, J. Li, X. Wang and Y. Zhang, Jiang L NL101 synergizes with the BCL-2 inhibitor venetoclax through PI3K-dependent suppression of c-Myc in acute myeloid leukaemia, *J. Transl. Med.*, 2023, **21**(1), 867, DOI: 10.1186/s12967-023-04312-0.

54 R. K. Kim, Y. Suh, K. C. Yoo, Y. H. Cui, H. Kim, M. J. Kim, I. G. Kim and S. J. Lee, Activation of KRAS promotes the mesenchymal features of basal-type breast cancer, *Exp. Mol. Med.*, 2015, **47**(1), e137, DOI: 10.1038/emm.2014.99.

55 W. Zhang, X. Shi, Y. Peng, M. Wu, P. Zhang, R. Xie, *et al.* HIF-1α promotes epithelial-mesenchymal transition and metastasis through direct regulation of ZEB1 in colorectal cancer, *PLoS One*, 2015, **10**(6), e0129603, DOI: 10.1371/journal.pone.0129603.

56 D. Kim and S. Rhee, Matrix metalloproteinase 2 regulates MDA-MB-231 breast cancer cell invasion induced by active mammalian diaphanous-related formin 1, *Mol. Med. Rep.*, 2016, **14**(1), 277–282, DOI: 10.3892/mmr.2016.5295.

57 N. A. Mathews and M. R. P. Kurup, In vitro biomolecular interaction studies and cytotoxic activities of copper(II) and zinc(II) complexes bearing ONS donor thiosemicarbazones, *Appl. Organomet. Chem.*, 2021, **35**, e6056, DOI: 10.1002/aoc.6056.

58 F. Bisceglie, N. Orsoni, M. Pioli, B. Bonati, P. Tarasconi, C. Rivetti, D. Amidani, S. Montalbano, A. Buschini and G. Pelosi, Cytotoxic activity of copper(II), nickel(II) and platinum(II) thiosemicarbazone derivatives: Interaction with DNA and the H2A histone peptide, *Metallomics*, 2019, **11**, 1729–1742, DOI: 10.1039/c9mt00166b.

59 C. A. Lipinski, F. Lombardo, B. W. Dominy and P. J. Feeney, Experimental and computational approaches to estimate solubility and permeability in drug discovery and development settings, *Adv. Drug Delivery Rev.*, 2012, **64**, 4–17, DOI: 10.1016/s0169-409x(00)00129-0.

60 M. A. Bakht, M. S. Yar, S. G. Abdel-Hamid, S. I. Al Qasoumi and A. Samad, Molecular properties prediction, synthesis and antimicrobial activity of some newer oxadiazole derivatives, *Eur. J. Med. Chem.*, 2010, **45**, 5862–5869, DOI: 10.1016/j.ejmech.2010.07.069.

61 C. A. Lipinski, B. W. Dominy and P. J. Feeney, Experimental and computational approaches to estimate solubility and permeability in drug discovery and development settings, *Adv. Drug Delivery Rev.*, 1997, **46**, 3–26, DOI: 10.1016/s0169-409x(00)00129-0.

62 M. A. Navia and P. R. Chaturvedi, Design Principles for Orally Bioavailable Drugs, *Drug Discovery Today*, 1996, **1**, 179–189.

63 D. F. Veber, S. R. Johnson, H. Y. Cheng, B. R. Smith, K. W. Ward and K. D. Kopple, Molecular properties that influence the oral bioavailability of drug candidates, *J. Med. Chem.*, 2002, **45**, 2615–2623, DOI: 10.1021/jm020017n.

64 P. Getreuer, L. Marretta, E. Toyoglu, O. Dömötör, M. Hejl, A. Prado-Roller, K. Cseh, A. A. Legin, M. A. Jakupec and G. Barone, Investigating the anticancer potential of 4-phenylthiazole derived Ru(ii) and Os(ii) metalacycles, *Dalton Trans.*, 2024, **53**, 5567–5579, DOI: 10.1039/d4dt00245h.

65 T. Bal and B. Ülküseven, Hydroxy and methoxy substituted N 1, N 4-diarylidene-S-methylthiosemicarbazone iron(III) and nickel(II) complexes, *Transition Met. Chem.*, 2004, **29**, 880–884.

66 *Stoe & Cie, X-AREA (Version 1.18) and X-RED32 (Version 1.04)*, Stoe & Cie, Darmstadt, Germany, 2002.

67 G. M. Sheldrick, SHELXT - Integrated space-group and crystal-structure determination, *Acta Crystallogr., Sect. A: Found. Adv.*, 2015, **71**, 3–8, DOI: 10.1107/S2053273314026370.

68 G. M. Sheldrick, Crystal structure refinement with SHELXL, *Acta Crystallogr., Sect. C: Struct. Chem.*, 2015, **71**, 3–8, DOI: 10.1107/S2053229614024218.

69 O. V. Dolomanov, L. J. Bourhis, R. J. Gildea, J. A. K. Howard and H. Puschmann, OLEX2: A complete structure solution,

refinement and analysis program, *J. Appl. Crystallogr.*, 2009, **42**, 339–341, DOI: **10.1107/S0021889808042726**.

70 T. Mosmann, Rapid Colorimetric Assay for Cellular Growth and Survival: Application to Proliferation and Cytotoxicity Assays, *J. Immunol. Methods*, 1983, **65**, 55–63, DOI: **10.1016/0022-1759(83)90303-4**.

71 *MIB Batch Molecule Processing, v2024.01, Nova Ulica, SK-900 26 Slovensky Grob*, Slovak Republic.